Third International Conference on Inverse Design Concepts and Optimization in Engineering Sciences (ICIDES-III), Editor: G.S. Dulikravich, Washington D.C., October 23-25, 1991.

APPLICATION OF DIRECT INVERSE ANALOGY METHOD (DIVA) AND VISCOUS DESIGN OPTIMIZATION TECHNIQUES

E. Greff+, D. Forbrich* and H. Schwarten**
Deutsche Airbus GmbH, Dept. of Aerodynamics, Bremen F.R.G.

ABSTRACT

A direct-inverse approach to the transonic design problem was presented in its initial state at ICIDES I. This paper reports further applications of the DIVA-method to the design of airfoils and incremental wing improvements and the verification in experiment. First results of a new viscous design code also from the residual correction type with semi-inverse boundary-layer coupling are compared with DIVA which may enhance the accuracy of trailing-edge design for highly loaded airfoils.
Finally the capabilities of an optimization routine coupled with the two viscous full potential solvers are investigated in comparison to the inverse method. The designer with expertise in specifying pressures can usually sort through certain design philosophies and off-design criteria more efficiently than an optimizer up to now.

I. INTRODUCTION

The application of CFD methods for analysis and design has been progressively increased in the past decade[1,2,3] but when it comes down to the global forces lift, drag and moment for transonic wings, let alone more complex configurations with pod interference, the general accuracy of wind tunnels remains unmatched. As cruise performance is the main driver for a transport aircraft design and the current designs in service already represent a high standard the designer has to meet very tight performance targets at a guarantee margin of 1-2% in drag.

This has to be achieved at limited budget and within a time frame of ~2.5 years during the definition phase through extensive iterations and repeated wind tunnel test loops. Increased quality requirements and complexity of the models, however, reduced the number of possible wing steps to 4-6. Hence greater emphasis was placed on inverse design concepts at DA based on a combination of a direct-inverse transonic design code with measured pressure distributions on complete configurations in order to derive incremental design improvements and performance estimates of high accuracy. Previous design codes in the 1970's have either worked with the hodograph equations[4,5], used direct optimization techniques[6] or tried the inverse approach for the full potential equation[7-10]. Hodograph methods are extremely difficult to use and limited to shock-free flows which in practice reveal adverse drag in off-design cases. Inverse methods that solve the Dirichlet problem need special treatment of the trailing-edge closure, which used to be a problem with earlier codes[9]. A variation of the nose shape[6] or tangential speed distribution along the a priori unknown arc length[11,12] can force closed profiles but in several cases the resulting pressure distribution is far off the desired one.

+ Head of Aerodynamic Design Department
* Research Engineer, Aerodynamic Design
** Research Engineer, Theoretical Aerodynamics

Third International Conference on Inverse Design Concepts and Optimization in Engineering Sciences (ICIDES-III), Editor: G.S. Dulikravich, Washington D.C., October 23-25, 1991.

A direct-inverse approach turns out to be more flexible in practical design, as it merely needs a specified pressure distribution and a starting geometry. Due to the modular structure of the computing concept - the residual between actual and specified pressures is determined by the use of an analysis code and the geometry corrected to minimize the residual - the transonic analysis code is exchangeable and flows with shocks and viscous interaction can be treated in the design cycle.

At ICIDES I the DIVA-method was presented in its initial state[13] and applied to several successful designs for airfoils and wings[14]. Further approaches to the viscous direct-inverse design were reported recently by Campbell[15] and Carlson[16] where even separated flows can be treated.

Higher order analysis codes that solve the Euler equations are already in use as to mention the ISES-Code by Drela[17] which is based on a coupling with an integral boundary layer formulation with a lag-dissipation closure. This code is very accurate in the analysis mode, the design modi available so far do not solve for an arbitrary pressure distribution. A starting geometry close to the desired one is necessary as the speed distribution on the leading edge is prescribed - a major disadvantage. Even Navier-Stokes-Codes are already offered as an analysis code in residual-correction design mode.

Efficient full-potential solvers coupled with semi-inverse boundary layer integral methods simulating wake curvature and thickness effects have demonstrated their accuracy with respect to pressure distribution and drag which is in the tolerance of different 2D windtunnels[18-21]. Three-dimensional analysis with full-potential or Euler solvers has experienced significant progress and even complex configurations with engine/jet-effects are being treated worldwide. Viscous effects however are mostly omitted or inaccurately modelled so far. Moreover the inverse formulation is an ill-posed problem.

For design purposes we therefore rely upon 2D-methods which can be used more rapidly and allow the designer to focus on key design parameters and quickly sort out different design philosophies. Some ingenuity is needed for the transfer to three-dimensional design, but this can be done by using an analogy method based on pressure distributions of a datum wing quite accurately.

II. THE DIRECT-INVERSE ANALOGY-METHOD (DIVA)

The two-dimensional transonic direct-inverse design method was presented in[13,14]. The DIVA uses an improved stream function method - based upon the work of Oellers[22] and Ormsbee and Chen[23] - to design an airfoil for a specified subsonic pressure distribution. The airfoil surface is replaced by a vortex sheet with linear variation of singularity strength between the surface node points (fig. 1), whereas the Ormsbee method used a constant strength.

The sum of a stream function for a parallel flow and the perturbation stream function of the vortex sheet is a constant on the airfoil surface. This is expressed in the following integral equation:

$$\psi_b + \frac{1}{2\pi} \oint_b \gamma(s) \ln r \, ds = Z \cdot U_\infty \cdot \cos \alpha - X \cdot U_\infty \cdot \sin \alpha \qquad (1)$$

Third International Conference on Inverse Design Concepts and Optimization in Engineering Sciences (ICIDES-III), Editor: G.S. Dulikravich, Washington D.C., October 23-25, 1991.

where ψ_b is the unknown constant on the body's surface. In order to solve the equation for the vorticity strength $\gamma(s)$ and ψ_b, the integral is approximated by a quadrature. The airfoil is divided into N-1 segments, where N is the odd number of panel node points. The singularity strength varies linear in between two node points. This yields a system of N simultaneous linear equations

$$\frac{1}{2\pi} \sum_{j=1}^{N} K_{ij} \cdot \gamma_j + \psi_b = Z_i \cdot U_\infty \cdot \cos \alpha - X_i \cdot U_\infty \cdot \sin \alpha \qquad (2)$$

i = control point.

The Kutta condition is

$$\gamma_1 + \gamma_N = 0 \qquad (3)$$

The influence of the wake is simulated by continuing the vortex sheet with constant γ downstream. It starts aligned with the bisector and turns slightly downstream into the direction of the oncoming flow.

A specified pressure distribution can be achieved by successive iteration of the ordinates Z_i, while the abscissae X_i remain constant. The ordinates Z_i^m of the mth iteration are determined by replacing the singularities of the (m-1)th iteration by the prescribed values γ_p:

$$Z_i^{(m)} = \frac{1}{\cos \alpha} \left(X_i \cdot \sin \alpha + \psi_b^{(m-1)} + \sum_{J=1}^{N-1} K_{ij}^{(m-1)} \cdot \gamma_p \right) \qquad (4)$$

The iteration ends if either the condition

$$\max_i \{\Delta Z_i\} = \max_i \{|Z_i^{(m)} - Z_i^{(m-1)}|\}$$

or

$$\max_1 \{\Delta C_{Pi}\} = \max_1 \{|C_{Pi}^{(m)} - C_{Pi}^{(m-1)}|\} \qquad (5)$$

is met.

As a first step for transonic design, the subsonic pressure distribution for a starting geometry is computed for M = 0 (M = Mach number). This wing section is then analysed in the high-speed region with the BGKJ program[24] coupled with a semi-inverse boundary layer method[18]. The target pressure distribution at transonic speed is compared with the BGKJ result and the differences (fig. 2) are scaled down to the subsonic regime according to a modified Kármán-Tsien rule. A new inverse step follows after modifying the subsonic pressure distribution. This iteration loop usually converges within 5-10 design cycles.

Sample design cases for inviscid and viscous design were reported[13] as well as applications to three-dimensional design. The purpose of this paper is to show successful applications and comparison with experiments for designs derived with the code and to present an improved viscous design code.

Third International Conference on Inverse Design Concepts and Optimization in Engineering Sciences (ICIDES-III). Editor: G.S. Dulikravich. Washington D.C., October 23-25, 1991.

III. APPLICATIONS OF DIVA-2D AND COMPARISON WITH EXPERIMENT

A typical task for a design engineer is to increase speed flexibility and for this purpose we tried to transpose the known characteristics of a datum airfoil designed for Cl = 0.565/M = 0.73 to M = 0.75 at constant lift and moment for a given thickness. Fig. 3 shows the computed result of the datum airfoil as well as the target which was slightly modified to keep local Mach numbers below 1.2. The required thickness was 11.5%, whereas the datum airfoil had 11.93%.

The measured pressures at off-design demonstrate the successful design. At this lift the new design shows nearly the same drag, whereas at lower lifts a significant improvement is demonstrated which is 5 drag counts (1 d.c. = 0.0001) better than the pure thickness effect. As the shock-strength at higher lifts turned out to be higher than expected, a geometry check was performed.

Whereas the maximum deviations in curvature are concentrated on the lower side and the nose region, the slope change on the upper surface seemed to be small (fig. 4). The computed iso-Mach contours however revealed a bucket in the sonic line. This is due to the coalescence of the compression waves reflected by the surface changing from convex to concave curvature. Such a coalescence results in the earlier formation of shock waves which was confirmed by Schlieren-pictures (fig. 5).

The new airfoil served as a fixed camber reference for a variable camber (VC) airfoil - a concept which was reported for example in[25]. A scheme of a system solution is given in fig. 6 using the existing high-lift system. The camber variation is achieved by small fowler motions, where the wheels of the flap carriage are guided by two individual tracks in such a way, that in VC-operation the flap body slides underneath the spoiler trailing edge. The control track and the flap upper surface have to be shaped such, that camber variation is performed with minor discontinuities in surface curvature.

As a consequence to this proposal - which allows only positive camber deflections - the design point is shifted to lower lifts where the wing is optimized with respect to minimum drag with relaxed off-design constraints. This will be the setting at low altitudes, low weight (medium range mission) and towards the end of cruise. At start of cruise, step climbs to higher altitudes or increased weight the lift demand is satisfied by discrete camber/fowler settings resulting in the envelope in fig. 6.

A first VC-airfoil was developed in reference to the fixed camber optimum airfoil mentioned above. For the design of the VC-airfoil criteria for a "VC-suited" pressure distribution were concluded which are illustrated in fig. 7. At the design point (Cl $\approx$ 0.45)

- the supersonic region should be confined to X/C $\approx$ 0.4 and terminated with a weak shock;
- the region close to Cp* should exhibit small gradients in order to guarantee a stable shock position in off-design conditions;
- the subsonic recompression gradients should not be larger than dCp/dx=3;
- the trailing edge recompression gradient should be degressive (Stratford-Type), which is benefical for the turbulence structure and hence reduces the friction drag;
- the balance of front loading and rear loading at the lower surface should be altered towards front loading to reduce the adverse effect of pitching moment.

Third International Conference on Inverse Design Concepts and Optimization in Engineering Sciences (ICIDES-III), Editor: G.S. Dulikravich, Washington D.C., October 23-25, 1991.

According to these criteria the airfoil was designed by DIVA.

A wind tunnel model with three VC-flap settings was tested. For each level of efficiency M*L/D the VC-airfoil demonstrated a greater flexibility in the Cl-M-plane and the maximum efficiency was increased by 12% (fig. 8). A calculation of the pressure distribution according to the VC-control law for four settings adjusted to the lift demand (fig. 9) incorporated the surface imperfections due to the discrete variation. The effects in pressure and drag are negligible which was confirmed by experiment.

In the framework of the national research program ZKP-TLFI natural laminar flow (NLF) investigations were performed. In comparison to a conventional airfoil the typical NLF design features are depicted in fig. 10. Laminar flow runs of 60% and 80% of the exposed wing area were assumed resulting in some 10% of aircraft cruise drag reduction. The required continuous acceleration imposes the problem of increased recompression gradients with potential separation and shock-wave boundary layer interaction upon the designer. In off-design conditions laminarity loss due to pronounced suction peaks and corresponding Tollmien-Schlichting instability or cross-flow instability with changing gradients versus lift may occur. A tool to shift the laminar bucket with increasing lift demand is available by the VC concept.

A first NLF-airfoil was designed with DIVA for a lift of 0.4 and M = 0.73 and tested. Fig. 11 shows a comparison of measurement and computation. The transition free drag is ~40% of the turbulent level and even the turbulent level turned out to be competitive to a conventional airfoil of same thickness.

Finally the survey of 2D-designs is concluded by an example for hybrid laminar flow control (HLFC). An arbitrary starting geometry was chosen (NACA 0008) and the result was established after 20 iterations (fig. 12, 13), a further proof of the versatility of the DIVA method.

IV. SAMPLE DESIGN CASE FOR 3D-DERIVATIVE DESIGN

In view of the difficulties of producing a design method for airfoils it is not surprising that no completely successful solutions for the three-dimensional transonic case are available. A combination of wind tunnel results of a datum aircraft with a direct-inverse design method seemed to be more promising though not satisfying from the scientists' viewpoint. Subsonic pressure distributions (up to M = 0.6) are used to design a zeroth iteration geometry by means of the subsonic inverse code. These sections include the subsonic cross-flow and viscous effects. If a transonic pressure distribution is then prescribed as target distribution, the DIVA method can design an airfoil representing the measured three-dimensional distribution when analysed with a two-dimensional direct code. This airfoil deviates from the actual section profile: it is an analogous numerically adapted profile.

Starting from this state, a redesigning of the wing is possible by improving the target pressure distributions in selected spanwise stations. The result is a new set of analogous profiles. The differences between the two sets of profiles have to be added to the datum wing sections and the new wing is defined. This may sound artificial, but is a quite reliable way to incorporate interference aspects in the design of a new wing. In[13] already two applications of this DIVA-3D were reported.

Third International Conference on Inverse Design Concepts and Optimization in Engineering Sciences (ICIDES-III), Editor: G.S. Dulikravich, Washington D.C., October 23-25, 1991.

A recent successful application was the validation of a trailing-edge modification on the Airbus A340 (fig. 14). A 3.75% chord extension combined with a camber increase was designed at the outboard engine position. The effect of the modification is a reduction of the lift break due to the engine and hence a gain in induced drag as well as a pressure drag improvement (fig. 15). The estimate in fig. 15 is in surprisingly good correlation with the subsequent test result.

V. AN IMPROVED DIRECT-DESIGN CODE WITH A HIGH ACCURACY VISCOUS TRANSONIC ANALYSIS CODE

The high accuracy of the viscous transonic analysis code SGW[19-21] was coupled with a new direct design method called REPAN, a name, which is an abbreviation of reverse panel method. The basic principle is the formulation as a minimization problem, which is adapted in the form

$$E = \sum_{i=1}^{M} \sigma_i [C_{pi}(\vec{a}) - C_{pi}^{target}]^2 \stackrel{!}{=} \text{Min} \qquad (6)$$

Thus we look for a profile, which fits best to the target-Cp-distribution at M discrete stations. The minimum of the merit function E is done with an algorithm due to Levenberg and Marquardt[26]. The geometry to be designed is given in terms of a set of design parameters $\vec{a}$, which specify the location and shape of the profile. Starting from an initial geometry the minimization is done by variing these parameters. To perform a minimization step, a matrix, relating pressure changes and parameter changes, has to be computed. This matrix is just the Jacobian of the transformation from parameters to pressures (= analysis code!). It is computed numerically.

The set of parameters, which specify the actual geometry, splits into two groups: global and local ones. The former include the chord angle and translation vector components between profiles for multi-element cases (fig. 16). They specify the location of the profiles without altering the shape. The profile shape is defined - separately for lower and upper side - by Bezier splines.

This technique uses a set of points $\vec{r}_i^B = (x_i^B, z_i^B), i = 1...n$ ('Bezier-knots', fig. 16) to define a curve with position vector $\vec{r}(t) = (x(t), z(t))$ by the parametric equation

$$\vec{r}(t) = \sum_{i=0}^{n} \vec{r}_i^B B_{n,i}(t) \qquad (7)$$

with

$$B_{n,i}(t) = \binom{n}{i} t^i (1-t)^{n-i} \quad , \quad 0 \le t \le 1 \qquad (8)$$

$\binom{n}{i}$ is the i^{th} binomial coefficient of order n.

The curve defined in this way has the following properties:

(i) The curve passes through the first and last Bezier knot for parameter values t = 0 resp. t = 1. This follows immediately from the definition, because we have

Third International Conference on Inverse Design Concepts and Optimization in Engineering Sciences (ICIDES-III), Editor: G.S. Dulikravich, Washington D.C., October 23-25, 1991.

$$B_{n,i}(0) = \begin{cases} 1 & i = 0 \\ 0 & i \neq 0 \end{cases}, \quad B_{n,i}(1) = \begin{cases} 0 & i \neq n \\ 1 & i = n \end{cases} \tag{9}$$

and the above sum reduces to

$$\vec{r}(0) = \vec{r}^{B}_{0} \; ; \; \vec{r}(1) = \vec{r}^{B}_{n} \tag{10}$$

(ii) Taking the derivative at t = 0 it follows, that

$$\dot{\vec{r}}(0) = n(\vec{r}^{B}_{1} - \vec{r}^{B}_{0}) \tag{11}$$

which is equivalent to

$$\left.\frac{dz}{dx}\right|_{t=0} = \frac{\dot{z}(0)}{\dot{x}(0)} = \frac{z^{B}_{1} - z^{B}_{0}}{x^{B}_{1} - x^{B}_{0}} \tag{12}$$

The derivative of the curve at the beginning is therefore given by the tangent of the first Bezier segment. An analogous result is valid at the endpoint t = 1.

These properties can be used to impose simple constraints on airfoil geometry. For airfoil design, $\vec{r}(t)$ represents a lower or upper side and t = 0|1 corresponds to the leading/trailing edge. The $\{x_i\}$ coordinates of the points of the initial airfoil are used to establish a corresponding set of parameters $\{t_i\}$; the Bezier ordinates - excluding the first and last one - z^{B}_{i}, i = 1, ...n-1 are the local design variables mentioned above. These will be determined in such a way, that the sum of squared pressure deviations is minimized.

As the airfoil is composed of two parts, some restrictions on Bezier knots have to be imposed to insure continuity of values, first and second derivative at the connection point i.e. the leading edge:

- The first Bezier knot is placed at the leading edge and held rigid.
- The second one has the same x-value as the first one: $x^{B}_{1} = x^{B}_{0}$. This serves for a normal tangent at the leading edge (see fig. 16).
- The ordinate z^{B}_{1} of the second Bezier knot is related to the curvature at the leading edge. This fact can be used in two ways: (1) relating the ordinates of the first Bezier Knots on the lower and upper side serves for continuous curvature with a value, determined by the design process, or (2) we can do a design with specified leading edge radius just by fixing the ordinates to their appropriate values. The design in fig. 19 is done with continuous but variable leading edge radius.

Similar conditions hold at the trailing edge. The last Bezier knot is placed at the last point of the lower resp. upper side and held rigid thereby keeping the trailing edge thickness constant. Additionally we could prescribe the tangent of the last Bezier segment thus performing a design with specified trailing edge angle.

The minimization of the sum of squared pressure deviations is done with an algorithm after LEVENBERG and MARQUARDT. It is an elegant method that combines the inverse Hessian method and the steepest descent method by introducing a factor ("Marquardt-factor"), which switches smoothly between these extremes.

Third International Conference on Inverse Design Concepts and Optimization in Engineering Sciences (ICIDES-III), Editor: G.S. Dulikravich, Washington D.C., October 23-25, 1991.

Far from the minimum (large factor) steepest descent steps are performed whereas approaching the minimum this factor is reduced automatically thus switching to inverse Hessian steps.

This method works very well in practice and has become the standard of nonlinear least squares routines. Details of the method may be found in[26]. Fig. 17 shows a simplified flow chart of the REPAN-design procedure.

In the past authors used the least squares method for solving the profile design. Labrujere[27] prescribes tangential velocities and uses Legendre polynomials for the shape description. He did not include global parameters. Bristow[28] used panel direction angles as design variables. He had to do additional Cp-control to achieve smooth profiles.

To formulate the inverse problem as a minimization problem has several advantages:

(1) As the inverse step is purely algebraic, each analysis code can be run in the reverse direction. The present method is optimized for coupling with panel codes - concerning calculation time - but any given code, even large scale ones as used in our test case two, can be used as well. But it should be mentioned, that additional code dependent research is required, to obtain solutions in reasonable time. Calculation time is the crucial point of this approach.

(2) The geometry definition includes the possibility of geometrical constraints, such as fixed trailing edge thickness, normal tangent at the leading edge, prescribed trailing edge angle. Curvature control during design process is possible by additional control of the turn-around angles at the Bezier-knots (fig. 16). This option is needed in critical cases only.

(3) From a practical point of view, flexibility in cases of partly unphysically specified target pressures, is the most important feature. Although we know, that constraint conditions are to be fulfilled by the Cp-target values[29], there are two situations, in which unproperly specified Cp's are unavoidable: measured Cp-distributions (because of measurement errors) and 2D-Cp-cuts from 3D-configurations (because of missing stagnation point). In such ill-posed cases we solve for the "nearest" profile in the least square sense. Additionally, if we have a guess of some unphysical target pressures, they can be "switched off" by setting the corresponding σ equal to zero. For small regions of the profile - where "small" means small with respect to the distance of Bezier-knots - we are allowed to do that, because the variation of a local parameter affects a reasonable part of the profile (in fact, the whole side, because Bezier-splines are nonlocal) and therefore the geometry is determined by the influence of nearby pressures, which are assumed to be correct. This has been proven to be helpful in the vicinity of the stagnation point and the trailing-edge region.

As a first validation example test case 2 from ref.[13] was chosen, which shows the design potential of a typical supercritical airfoil with rear loading. By means of a calculation with the BGKJ code including semi-inverse boundary-layer coupling, the pressure distribution in fig. 18 was obtained. Considerations concerning a reduction of rear loading led to the modified target distribution also depicted in fig. 18.

In the case of DIVA a liquid surface is designed where the displacement thickness has to be subtracted whereas the REPAN code solves directly for the solid geometry by applying viscous iteration in the analysis. The geometry modifications delivered from both codes are given in fig. 19 as well as a comparison of

the last REPAN iteration with respect to the target pressures which is satisfactorily matched. The redesigned airfoils are quite similar at first sight but the REPAN airfoil does not meet the required thickness (12.55% instead of 12.93%) and a significant deviation of the trailing-edge camber can be noticed. This corresponds to not properly specified trailing-edge thickness. As mentioned above this quantity is held fixed during design process. Cp-control is done everywhere except at three stations near stagnation point.

In order to compare the two different designs, the airfoils were calculated for the same lift and Machnumber with the BGKJ code incl. boundary layer iteration. While the agreement with the target distribution (fig. 20) for the DIVA airfoil is still quite good the REPAN airfoil shows a larger deviation. This is due to the local change at the trailing-edge and corresponding higher angle of attack for a given lift. At the design point the DIVA airfoil shows 1.5 d.c. less drag and a 43% reduction in pitching moment with respect to the datum airfoil. The REPAN airfoil however exhibits 2.5 d.c. excess drag despite the reduced thickness. If the thickness is scaled to the target value additional 2 d.c. have to be added; i.e. that the improvement at lower lifts in fig. 20 is diminished. Hence it can be concluded that at the present state further investigations devoted to the accuracy of the trailing-edge region seem to be necessary in order to enhance the viscous design modus.

VI. Application of a Numerical Optimization Routine

The design methods described so far require an experienced designer with physical insight into the trade-offs of the pressure distribution he specifies. But what is the ideal pressure distribution with respect to different objectives under practical constraints? A further class of design methods using optimization routines may give an answer to this.

Coupling of a gradient method with two transonic aerodynamic analysis codes
In an optimization process a so-called 'objective function' $F(\bar{X})$ is to be minimized (or maximized) subject to a set of (m) given constraints $G_j(\bar{X}) \leq 0$, $j = 1,m$ with $\bar{X}$ being the vector of the design variables.

Relating to the design of an airfoil the variables would have to define the airfoil shape while the objective function would be a characteristic of this airfoil, for example the drag coefficient Cd, at a given design point. To keep the design inside certain boundaries and allow the optimization code to converge faster some constraints on other airfoil characteristics such as lift, pitching moment etc. or geometrical constraints like the thickness, camber, trailing edge thickness should be imposed.

Though a lot of different optimization techniques can be applied to approach this design problem it is evident that, among the existing nonlinear minimization routines, the Vanderplaats gradient method[6,30,31,35] is the most widely used[32,33,34,36].

This optimization code called CONMIN (Constrained Function Minimization) is part of COPES, a Control Program for Engineering Synthesis. In this code the strategy, one-dimensional search direction and optimizer can be chosen by the user and adapted to a certain problem.

Fig. 21 shows the principle of the design process. The optimization direction finding process of COPES is illustrated for the two-variable case. First each

Third International Conference on Inverse Design Concepts and Optimization in Engineering Sciences (ICIDES-III), Editor: G.S. Dulikravich, Washington D.C., October 23-25, 1991.

component of the design variable vector $\bar{X}$ is varied starting from $\bar{X}^\circ$ (initial design variables) and leading to a gradient $\nabla F(\bar{X}^\circ)$. This could be taken as the search direction $\bar{S}$ but because of convergence problems for nonlinear functions the "method for conjugate directions" is being prefered. In this case $\bar{S}$ is calculated from the gradient and the last search direction by

$$\bar{S}^q = -\nabla F^q + |\nabla F^q|^2 \,/\, |\nabla F^{q-1}|^2 \cdot \bar{S}^{q-1} \qquad (13)$$

If the design comes in contact with a constrained region the search direction $\bar{S}$ is found taking the gradient ∇G_j of the active constraint and ∇F of the objective function. In addition a "push off factor" is used to direct the search vector in the region where the feasible sector (allowed designs) and the usable sector (designs with improved objective function) overlap. This region is called the usable feasible sector. Since every iteration step needs n+3 analysis, i.e. about 10n+30 calculations for one design, which has to be done by a precise, time consuming (therefore expensive) aerodynamic analysis code, COPES offers another design mode to approach these problems. Here the objective function and the constraints are developed as second order Taylor series expansions :

$$F(\bar{X}) = F^\circ + \Delta\bar{X}^T\nabla F + 1/2\Delta\bar{X}^T[H]\,\Delta\bar{X}$$

$$G_j(\bar{X}) = G_j^\circ + \Delta\bar{X}^T\nabla G_j + 1/2\Delta\bar{X}^T[H]_j\Delta\bar{X} \qquad (14)$$

with
$\Delta\bar{X} = \bar{X}-\bar{X}^\circ$
$F = F(\bar{X})$ at $\bar{X}^\circ$
$[H]$ = Hessian Matrix
∇F = vector of first partial derivatives

Using this mode of the code assures accelerated convergence because data calculated in one iteration step are still known in another step, which is not the case for the standard design mode. Also only one exact analysis is needed for every iteration, whereas the first Taylor series expansion requires $1+n+n\cdot(n+1)/2$ additional analysis in this approximation mode. So the method should be used for less than twenty design variables to be more efficient than the standard finite difference mode. Through the Taylor series the user is also able to prescribe a solution and accelerate the convergence of the code even more if he has some good designs to start from. In fig. 21 the approximation mode is depicted.

An airfoil shape can be described by the design variables either in the form of an analytical function or a function of aerodynamic origin, i.e. an airfoil library (fig. 21) or so-called aerofunctions. The analytical functions describe an airfoil by polynomials of higher order, which leads to a large number of design variables or problems of fitting the polynomials together if the airfoil is divided into different sections. Also some unrealistic shapes may occur because the solutions are purely mathematical.

In order to start the process the analytical functions are fitted on an initial shape and coefficients are obtained. These coefficients together with the Mach-number, the angle of attack (or the lift coefficient) and the given set of constraints are needed by the program to optimize the objective function. The coefficients are the design variables being perturbed by the optimizer to reach an optimal design. A new shape is prescribed by the linear combination

$$\bar{Y} = \bar{X}_0 + X_1\bar{F}_1 + X_2\bar{F}_2 + \ldots + X_n\bar{F}_n \qquad (15)$$

with $(X_j,\ j = 0,n)$ design variables (shape coefficients)
$(F_j,\ j = 1,n)$ vector with analytical shape functions

With respect to the orders of the analytical function n, a compromise has to be found between a large number of variables and a good approximation of an airfoil shape. The last also depends on the type of function that will be used, since some functions tend to reveal oscillations even at higher polynomial orders. Generally the order should not exceed twenty on the whole airfoil because the analysis especially with a viscous code will be too expensive.

Similar to the preceding definition functions of aerodynamic origin are applied by superposition of different airfoil shapes from an airfoil library with a linear combination (see fig. 23). In this case the Y-coordinates (shape functions) are defined numerically and not by analytical functions. By adding special airfoils to the library that fulfil some desired constraints it is possible to impose these constraints on the optimized shape without giving this information to the optimization code. Therefore these constraints do not have to be evaluated and checked for their influence on the objective function during every design loop, which means saving time.

Another type of functions with aerodynamic origin are quoted as "aerofunctions" in some references[32,36]. Here pressure distribution shape functions are superimposed on an initial pressure distribution and the perturbations are related to different airfoil shapes. This also promises to provide some realistic shapes as optimum solutions. In the present design task an airfoil library is used to define the shape but later the program should be expanded with regard to analytical functions.

The viscous BGKJ-code[18,24] and the SGW-code[19-21] are both coupled with COPES. Especially the latter provides a high accuracy analysis tool to calculate coefficients describing the characteristics of an airfoil at the design point. This is needed to make the direct design competitive against the inverse design methods.

Test cases

To validate the successful coupling a testcase from Vanderplaats[31,35] is being calculated with the BGKJ-code as analyser. With a given set of four NACA airfoils and two basic shapes to impose geometric conditions an airfoil with maximum lift for $M_\infty = 0.1$ and $\alpha = 6°$ should be found that satisfies the constraints mentioned in fig. 22.

In this figure the initial airfoil, the reference airfoil and the optimized airfoil after 42 iterations without and 17 iterations with Taylor series expansion are compared. Despite the different analyser the result differs only slightly from the reference, whereas the result without Taylor series expansion is still not converged.

For the second test case a library of six transonic airfoils is given to redesign the VA2 airfoil at $M_\infty = .73$, Cl = .552 for minimum drag. Since the design was already performed by the DIVA-code with the BGKJ-code as analyser the role of constraints and the influence of the library on the design should be investigated.

Fig. 23 illustrates the set of airfoils and constraints for which the converged solution after 30 iterations does not give a realistic shape comparable with the one designed by DIVA. This is also the case if the constraints are relaxed or a pressure gradient is prescribed. Only if the Cm-constraint is omitted the optimizer converges after 25 iterations showing an airfoil that resembles more the VA2 type, especially concerning the rear loading. The pressure distribution

Third International Conference on Inverse Design Concepts and Optimization in Engineering Sciences (ICIDES-III), Editor: G.S. Dulikravich, Washington D.C., October 23-25, 1991.

emphasizes this circumstance. A solution close to the DIVA optimized airfoil however can be found if this airfoil is included in the library. Therefore it can be concluded that for the given task the airfoil library is not sufficient to design an airfoil as good as the DIVA airfoil, for which off design aspects are also considered.

For the third test case COPES is coupled with the SGW-code to redesign the VA7 airfoil. This basic VC-airfoil should be optimized with respect to minimum drag at the design point M = 0.74, Cl = 0.45 and constant thickness. The optimization result after 19 iterations is depicted in fig. 24. Though the changes are only moderate a drag reduction of one count is reached. Again the library of four airfoils (see fig. 24) does not allow a better result starting from the VC-airfoil with only small changes in the shape for every design iteration.

Nevertheless this combination of COPES and SGW as analyser promises to work more efficient if analytical functions are used to describe the airfoil.

VII. Conclusion

Applications of the direct-inverse analogy-method (DIVA) for the design of supercritical airfoils and wing modifications have been presented and verified by experiment.

The method yields results with high accuracy even for flows with strong shocks. It is as simple as possible from the user's point of view and merely needs a pressure distribution as input. The influence of the starting geometry (i.e. nose shape) is negligible.

An application to three-dimensional design is possible, provided an initial wing shape and pressure measurements are available. Incremental improvements of wing performance may be assessed with an accuracy less than 1 per cent.

Due to the modular structure of the computing concept, the transonic code is exchangeable, and improved codes can be implemented. So the DIVA method is a comprehensive tool for practical wing design. Future applications by using 3D-Euler results including viscous corrections instead of measurements are planned in order to obtain further refinements of the design before testing it.

A new residual correction design code with complete semi-inverse boundary layer iteration in the design cycle was presented which may enhance the accuracy of trailing-edge design for highly loaded airfoils. Further work in this field is envisaged.

Finally applications of a numerical optimization routine coupled with two viscous full potential solvers were discussed. A significant dependence of the results upon the airfoil library to be composed was found. A more general geometry description seems of paramount interest. However the designer with expertise in specifying pressures may win hands down in this competition.

VIII. REFERENCES

1. L.R. Miranda, **'Application of computational aerodynamics to airplane design'**, J. Aircraft, **21** (6)(1984).
2. P. Rubbert and M. Goldhammer, **'CFD in design: An airframe perspective'**, AIAA paper No. 89-0092 (1989).
3. R.C. Lock, **'Aerodynamic design methods for transonic wings'**, Aeron. Journal, Jan. 1990, 1-16.
4. G.Y. Nieuwland, **'Transonic potential flow around a family of quasi-elliptical aerofoil sections'**, NLR-TR-T.172, National Lucht- en Ruimtevaart Laboratorium, Amsterdam (1967).
5. F. Bauer, P. Garabedian and D. Korn, **'A Theory of Supercritical Wing section, with Computer Programs and Examples'**, Springer- Verlag, 1972.
6. R.M. Hicks, E.M. Murman and G.N. Vanderplaats, **'An assessment of airfoil design by numerical optimization'**, NASA TM X-3092 (July 1974).
7. L. Carlson, **'Transonic airfoil design using cartesian coordinates'**, NASA-CR 2578 (April 1976).
8. T.L. Tranen, **'A rapid computer aided transonic airfoil design method'**, A.I.A.A. Paper No. 74-501 (June 1974).
9. G.B. Mc Fadden, **'An artificial viscosity method for the design of supercritical airfoils'**, NASA-CR-158840 (1979).
10. H. Sobieczky, **'Supercritical airfoil and wing design'**, Ann. Rev. Fluid Mech., **16**, 337-363 (1984).
11. G. Volpe, **'The inverse design of closed airfoils in transonic flow'**, A.I.A.A. paper 83-0504.
12. G. Volpe and R.E. Melnik, **'Method for designing closed airfoils for arbitrary speed distributions'**, J. Aircraft, 1986, **23**, (10), 775-782.
13. E. Greff and J. Mantel, **'An Engineering Approach to the inverse transonic wing design problem'**, Comm. in Appl. Num. Meth., Vol. 2, (1986), 47-56.
14. H. Sobieczky, **'Research on inverse design and optimization in Germany'**, Proc. of the 2. Int. Conf. on Inv. Design Concepts in Eng. Sciences, Oct. 26-28, 1987, Penn-State-University, Pennsylvania
15. R.L. Campbell and L.A. Smith, **'Design of transonic airfoils and wings using a hybrid design algorithm'**, SAE-paper No. 871756, (1987).
16. L.A. Carlson, **'A direct-inverse method for transonic and separated flows about airfoils'**, NASA CR-4270, Jan. 1990.
17. M. Drela and M.B. Giles, **'ISES - a two-dimensional viscous aerodynamic design and analysis code'**, AIAA-paper No. 86-0424, (1987).
18. P. Thiede, G. Dargel and E. Elsholz, **'Viscid-inviscid interaction analysis on aerofoils with an inverse boundary layer approach'**, in Recent Contribution to Fluid Mechanics (Ed. W. Haase), Springer-Verlag, 1982.
19. G. Dargel and P. Thiede, **'Viscous transonic airfoil flow simulation by an efficient viscous-inviscid interaction method'**, AIAA paper 87-0412, Jan. 1987.
20. T. Holst, **'Viscous Transonic Airfoil Workshop'**, AIAA paper 87- 1460, June 1987, Honolulu.
21. J. Mertens, K.D. Klevenhusen and H. Jakob, **'Accurate transonic wave drag prediction using simple physical models'**, AIAA Journal, **25**(6)(June 1987), 799-805.
22. H.J. Oellers, **'Die inkompressible Potentialströmung in der ebenen Gitterstufe'**, WGL Jahrbuch, 1962.
23. A.I. Ormsbee, **'Multiple element airfoils optimized for maximum lift coefficient'**, J. Aircraft, **10**(12)(Dec. 1972).

24. F. Bauer, P. Garabedian, D. Korn and A. Jameson, **'Supercritical wing sections I, II, III'**, Lecture Notes in Economics and Mathematical Systems, **66**(1972), **108**(1975), **150**(1977), Springer- Verlag, Berlin/Heidelberg/New York.
25. E. Greff, **'Aerodynamic Design and Integration of a Variable Camber Wing for a New Generation Long/Medium Range Aircraft'**, ICAS-88-2.2.4, Jerusalem/Israel.
26. P.E. Gill, W. Murray and M.H. Wright, **'Practical optimization'**, Academic Press, Inc., 1981.
27. Th.E. Labrujere, **'Multi-element airfoil design by optimization'**, ICAS Proceedings, Volume 1978, 305-312.
28. D.R. Bristow, **'A new surface singularity method for multi-element airfoil analysis and design'**, AIAA-paper No. 76-20,(1976), 14th Aerospace science meeting.
29. G. Volpe and R.E. Melnik, **'Role of constraints in inverse design for transonic airfoils'**, AIAA Journal, **22**(12), (Dec. 1984), 1770-1778.
30. G.N. Vanderplaats, **'CONMIN-A Fortran Program for Constrained Function Minimisation'**, NASA TM X-62, 282, August 1973.
31. G.N. Vanderplaats and R.M. Hicks, **'Numerical airfoil optimization using a reduced number of design coordinates'**, NASA TM X-73, 151, July 1976.
32. J. Reneaux and J.J. Thibert, **'The use of numerical optimization for airfoil design'**, AIAA-paper No. 85-5026, (1985).
33. P. Krantz, S.G. Hedman, **'Airfoil Optimization'**, J. Aircraft, 1986, **23**(5), 355-335.
34. K.-W. Bock, **'Aerodynamic Optimization'**, ICAS-88-4.4.1, Jerusalem/Israel.
35. G.N. Vanderplaats, **'Efficient Algorithm for numerical airfoil optimization'**, J. Aircraft, **16**(12), (Dec. 1979).
36. P.V. Aidala, W.H. Davis, W.H. Mason. **'Smart aerodynamic optimization'**, AIAA-paper No. 83-1863, (1983).

Third International Conference on Inverse Design Concepts and Optimization in Engineering Sciences (ICIDES-III), Editor: G.S. Dulikravich, Washington D.C., October 23-25, 1991.

IX. FIGURES

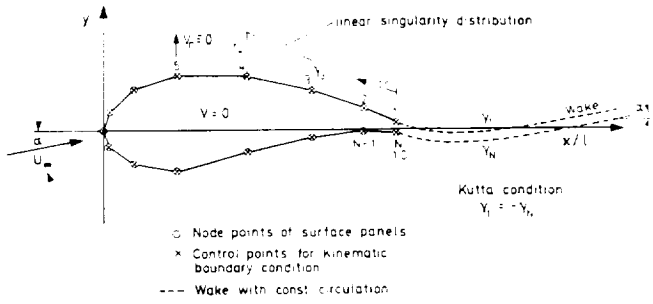

Fig. 1 Singularity Distribution for Subsonic Inverse Code

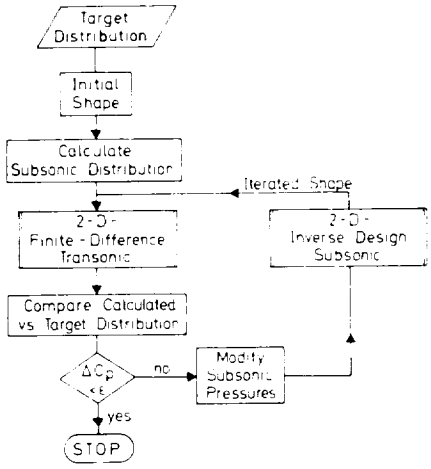

Fig. 2 Direct Inverse Analogy (DIVA) Method

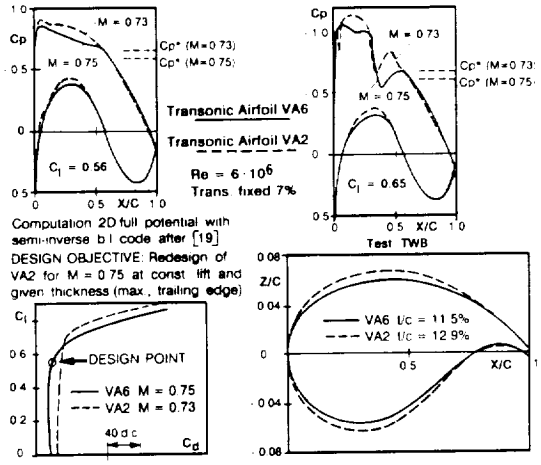

Fig. 3 Redesign of VA2 Airfoil at Increased Speed

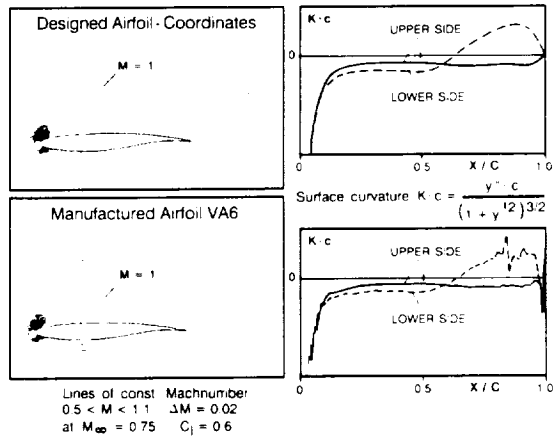

Fig. 4 Effect of Manufacture Tolerances

Fig. 5 Schlieren - Picture Showing Coalescence of Compression Waves at M = 0.75; C_l = 0.602

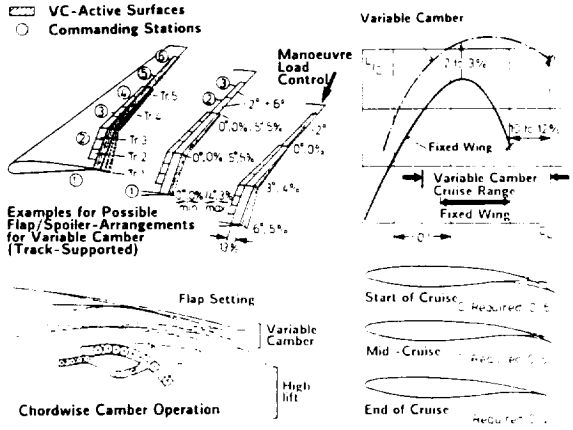

Fig. 6 Principle of Variable Camber Operation

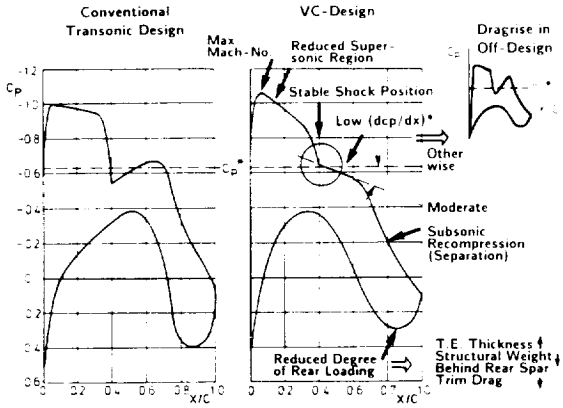

Fig. 7 Considerations on Properly Prescribed Pressure Distributions for Variable Camber Airfoil

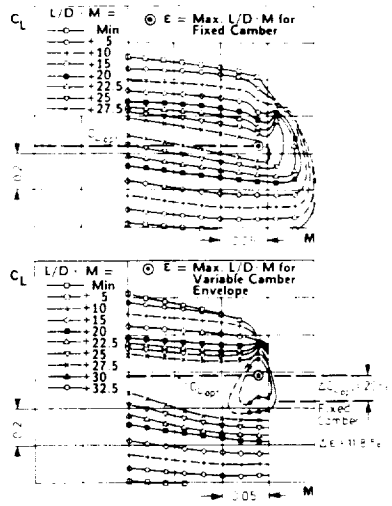

Fig. 8 Aerodynamic Efficiency of the VC - Airfoil in Reference to the Fixed Camber Design VA6

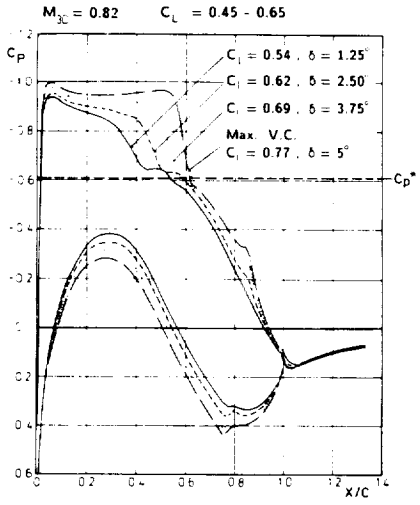

Fig. 9 Pressure Distribution of VC - Airfoil with Increasing Lift

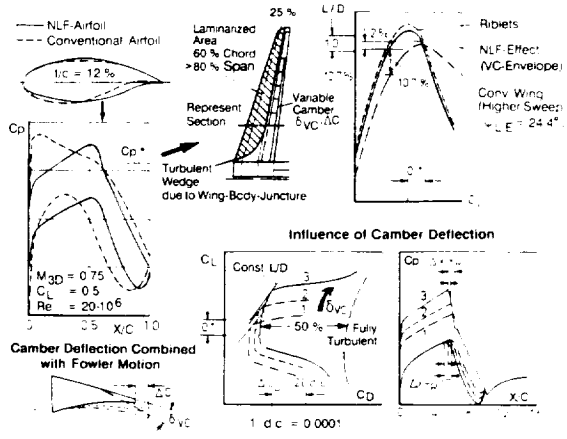

Fig. 10 Principle and Potential of NLF - Technology

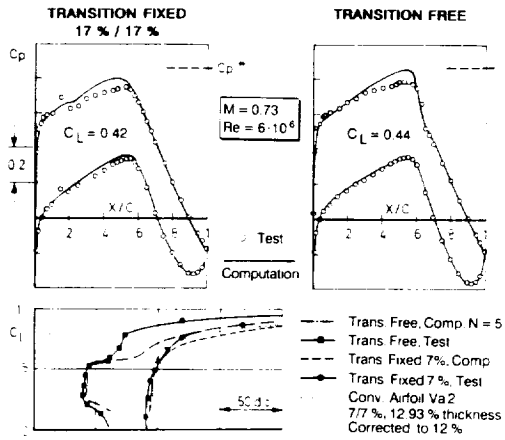

Fig. 11 Comparison of Experiment / Theory for NLF - Airfoil

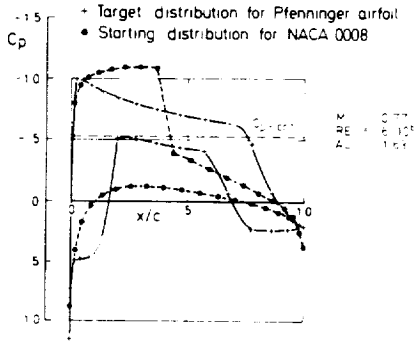

Fig. 12 Design of HLFC - Airfoil Target Distribution

Third International Conference on Inverse Design Concepts and Optimization in Engineering Sciences (ICIDES-III), Editor: G.S. Dulikravich, Washington D.C., October 23-25, 1991.

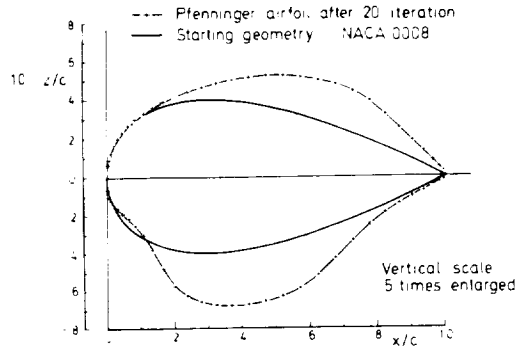

Fig. 13 Design of HLFC - Airfoil
Comparison of Iterated Shape With Starting Shape

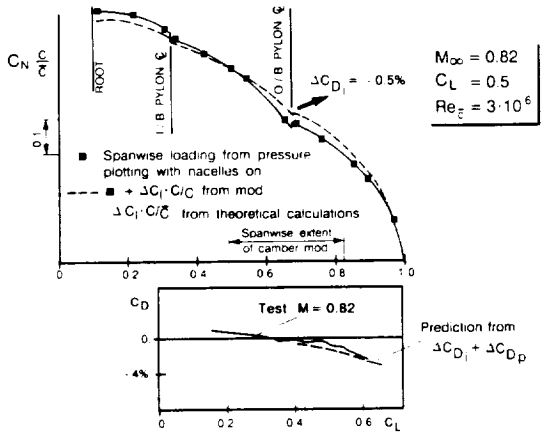

Fig. 15 Efficiency of Drag Prediction Using DIVA - 3D

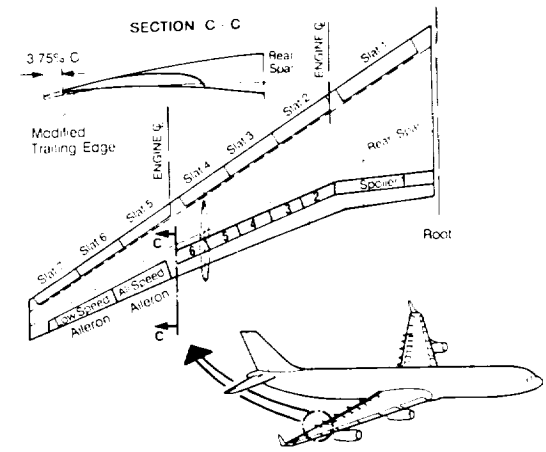

Fig. 14 Trailing Edge Extension on Airbus A 340

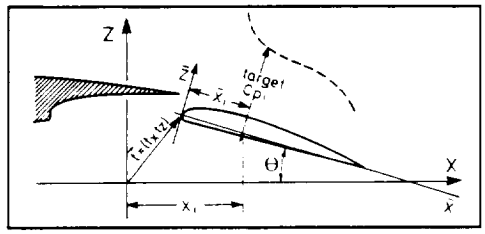

Global parameters (t_X, t_Z, Θ) for flap design

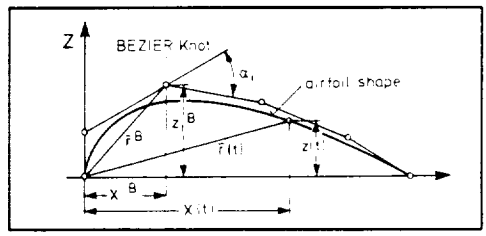

Local parameters as ordinates of defining BEZIER-polygon

Fig. 16 Local and Global Parameters of Defining BEZIER Polygon

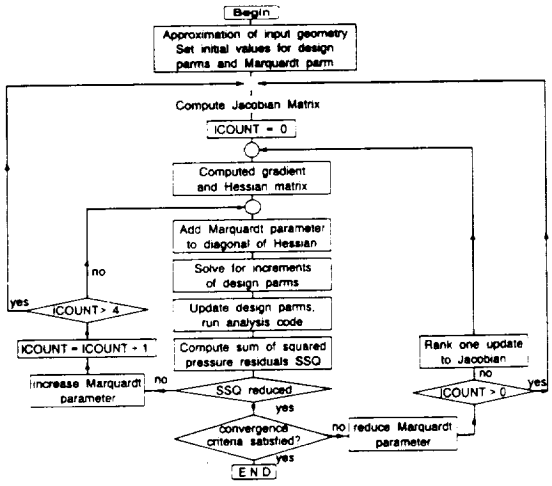

Fig. 17 REPAN Flow Chart

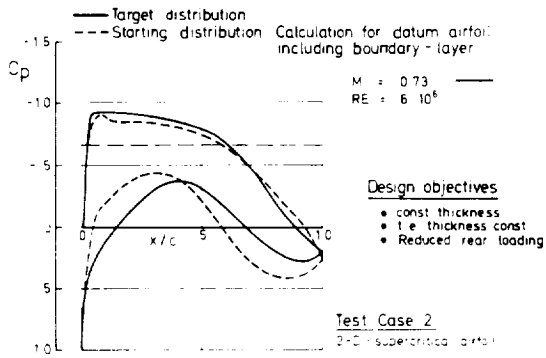

Fig. 18 Testcase 2 for 2D - Viscous Design

Third International Conference on Inverse Design Concepts and Optimization in Engineering Sciences (ICIDES-III), Editor: G.S. Dulikravich, Washington D.C., October 23-25, 1991.

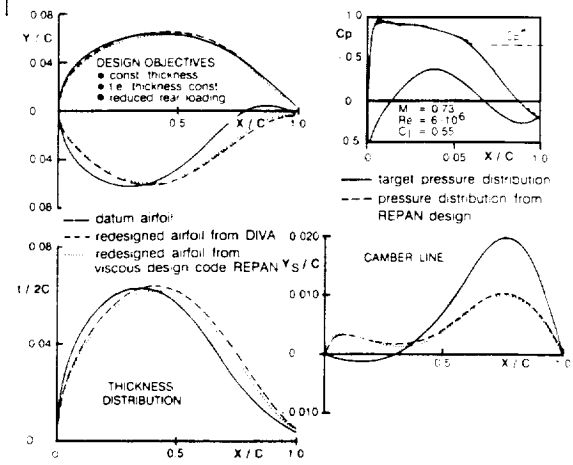

Fig. 19 Geometry Modifications on a Supercritical Airfoil

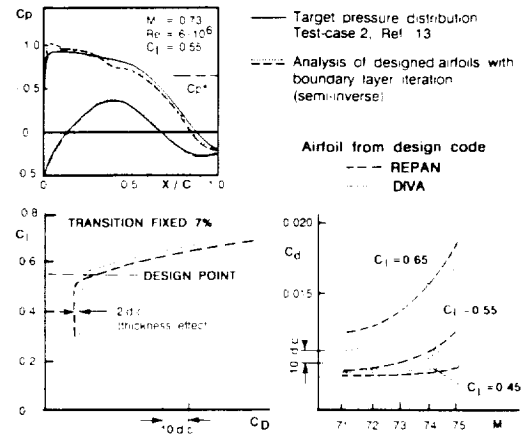

Fig. 20 Accuracy of 2D - Viscous Design

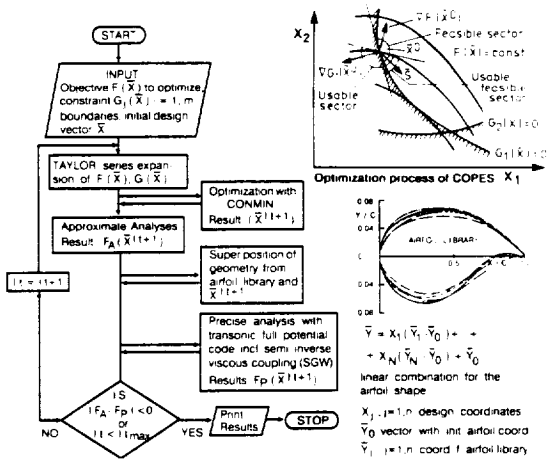

Fig. 21 Principle Flowchart of the Optimization Process with COPES

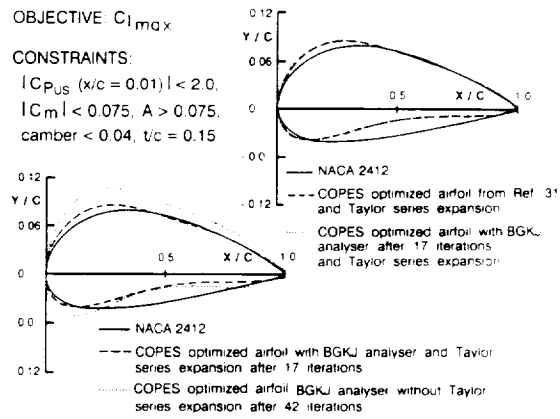

Fig. 22 Verification of the COPES - BGKJ - Coupling with a Testcase from Ref. 35

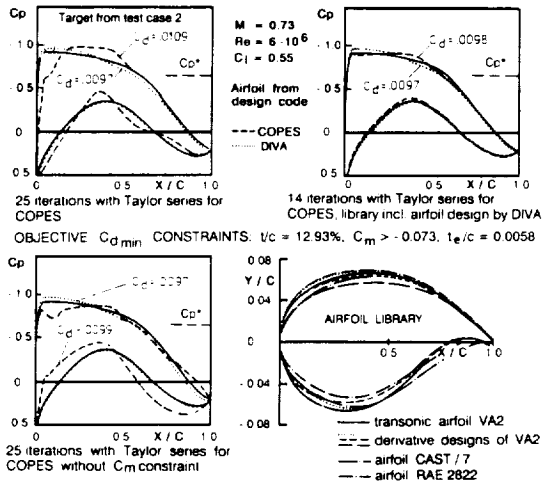

Fig. 23 Role of Constraints and Airfoil Library

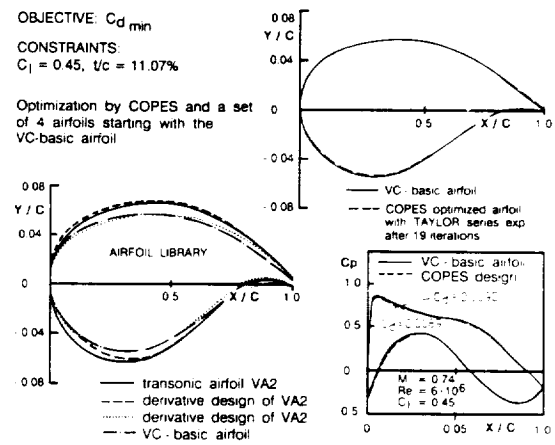

Fig. 24 Application of COPES for Optimization of a VC - Airfoil